



Wear properties and synthesis of CrFeNiMoTi high entropy alloy coatings produced by TIG process

Serkan Islak^{a*}, Özkan Eski^a, Vahdettin Koç^b & Cihan Özorak^c

^aMechanical Engineering, Faculty of Engineering and Architecture, Kastamonu University, Kastamonu 37150, Turkey

^bVocational High School of Technical Sciences, Adiyaman University, Adiyaman 02000, Turkey

^cMetallurgical and Materials Engineering, Faculty of Engineering and Architecture, Kastamonu University, Kastamonu 37150, Turkey

Received: 23 August 2017 ; Accepted: 17 January 2019

The aim of this study is to investigate wear and microstructure properties of CrFeNiMoTi high entropy alloy coating produced by using tungsten inert gas (TIG) process on the medium carbon steel. The coatings have been compared in terms of their phase composition, microstructure, and hardness. Phase compound and microstructure of coating layers have been examined by using X-ray diffractometer (XRD), scanning electron microscope (SEM), and optical microscope (OM). The images show that the coatings have consisted of the cladding zone, interface zone, and heat affected zone. Also, the microstructure of the coating has been mainly composed of dendrite and discontinuous interdendritic segregation. The surface microhardness of this high entropy alloys up to 450 HV_{0.3}, has been about 2.5 times as the substrate. The wear behaviour of the specimens has been compared through dry sliding wear tests under the same conditions. Average coefficient of friction values of the high entropy alloy (HEA) coating has been obtained at relatively low levels.

Keywords: HEA coating, CrFeNiMoTi, TIG process, Microstructure, Wear

1 Introduction

High entropy alloys (HEAs) have captivated increasing attentions owing to their unique compositions, microstructures, and adjustable properties in recent years. They are defined as solid solution alloys that contain more than five principal elements in equal or near equal atomic percent (at.%). Normally, the atomic fraction of each component is greater than 5 at.%. The multi-component equi-molar alloys should be located at the centre of a multi-component phase diagram and their configurational entropy of mixing reaches its maximum value for a solution phase^{1,2}. HEAs normally have relatively simple phases: a body-centred cubic (bcc) solid solution and/or a face-centred cubic (fcc) solid solution with or without nano-precipitates^{3,4}.

In recent years, surface coating techniques have been successfully applied on different substrates to provide a better surface property^{5,6}. The most common surface coating techniques are vapour deposition (PVD and CVD), sol-gel, electrolytic coating, and hard-facing process (welding and thermal spray)⁷. Hard-facing primarily involves deposition of a hard and wear-resistant material to the specific areas of the

surface of the components by any of the techniques such as welding and thermal spraying⁸.

Welding cladding techniques rely on a metallurgical bond between the coating layer and the substrate. Among the weld cladding procedures, tungsten inert gas (TIG) surfacing process is a cost-effective approach applied when reactive materials (as coatings or substrates) are involved⁹⁻¹². In this method, substrate surface and powder or hard filler wire used for coating were melted down by using arc source and then solidified, which resulted in the formation of a new cladding layer^{13,14}. In this study, CrFeNiMoTi high entropy alloy coating was produced by using TIG. TIG process was selected because it is a cost-effective approach for melting-based coatings. Phase compound, microstructure, hardness and wear properties of the coating were examined.

2 Experimental Studies

In coating processes, the substrate material used was a 20 x 10 x 80 mm³ AISI 1040 steel. In order to place coating powders, holes with an 8-mm width, a 1.5 mm depth and a 60-mm length were drilled on substrates. Before TIG method, surfaces of the steel material were cleaned by using acetone. The equiatomic Cr, Fe, Ni, Mo and Ti of the powder

*Corresponding author (E-mail: serkanislak@gmail.com)

mixture were prepared by mechanically mixing commercially pure elemental powders. The powders were placed in holes over substrate after being mixed with an amount of bonding. Then, specimens were dried at 100 °C for 30 min. Figure 1 shows schematically the operating principle of TIG process system. The TIG process parameters used in this study were listed as follows: working voltage of 20 V, working current of 160 A, the nozzle's travel speed of 72 mm/min, the shielding gas flux (Ar) of 12 L/min, electrode type W-%2 ThO₂, and the electrode diameter of 2.4 mm.

Metallographic specimens were prepared normally by mounting in resin, grinding on water-lubricated silicon carbide papers, and polishing with diamond paste down to 1 μm finish. Phases of the specimens were identified by using Bruker D8 Advance XRD device model diffractometer with Cu-Kα radiation ($\lambda=1.5418 \text{ \AA}$). The scan ranging from 3° to 90°, with a step size of 0.02° 2θ and counting time of 0.5 s was applied at each step. The microstructure of the coating was evaluated by using SEM (FEI QUANTA 250 FEG) and optical microscope (Olympus GX41). Chemical composition of the alloys was done by means of energy dispersive spectrometry (EDS) in SEM. Microhardness measurements were carried out by using Shimadzu HVM-2 model digital microhardness tester. The load was applied for 15 s and at 300 g. For wear tests of the substrate and the coating, reciprocating mode and Ball-on-Flat geometry were used on a UTS Tribometer device (ASTM G133 standard). All tests were carried out with 10 N, 15 N and 20 N normal loads in order to obtain 5 cm/s wear rate and 300 m sliding distance. Wear properties were evaluated sliding a 100Cr6 steel 6 mm diameter ball against the coated specimens. The tests were carried out under dry conditions and the medium used was air. Worn surfaces were

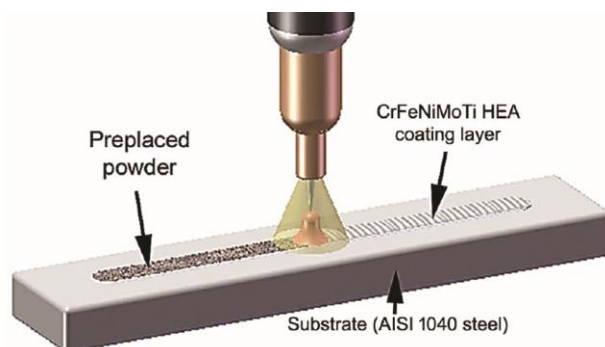


Fig. 1 — Schematic diagram of the TIG process system.

examined based on SEM and EDS analysis of specimens. In order to determine the wear depth, the wear track profiles were recorded by using a profilometer and then calculated by using the superimposed profiles.

3 Results and Discussion

3.1 Microstructure

Figure 2 shows the cross-sectional microstructure of the CrFeNiMoTi HEA coating. The rapid directional solidification can be observed at the bonding area of the coating where the growth direction of columnar grains is perpendicular to the interface, as shown in Fig. 2a. Dendritic microstructure formed partly in the coating layer (Fig. 2b). The reason for formation of the partially dendritic solidification structure may be that multiple elements have different solidification properties.

It is very important to obtain element distribution in coating in order to enhance mechanical properties of the materials. Figure 3 shows images of MAP

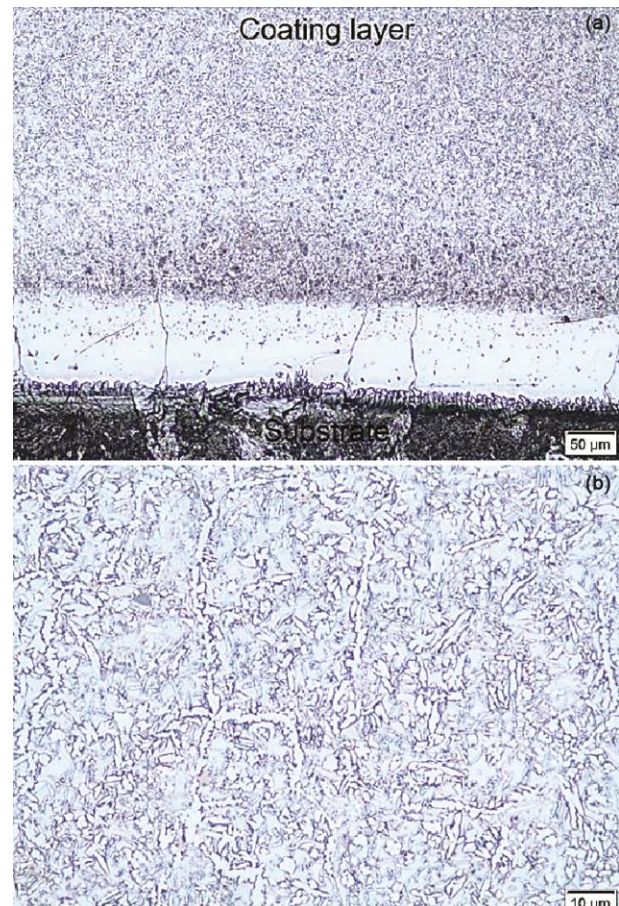


Fig. 2 — Optical images of coating (a) General view and (b) Center of the coating.

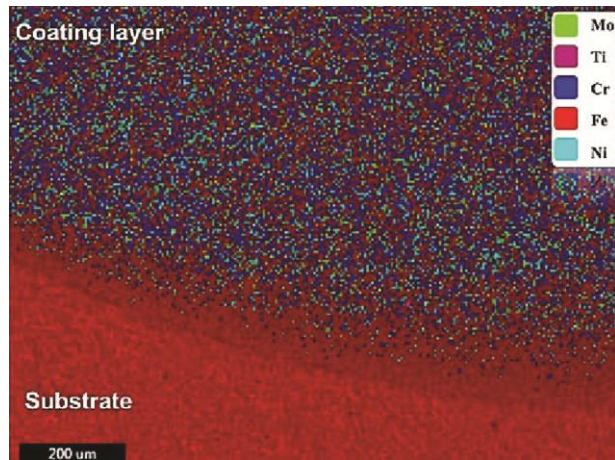


Fig. 3 — MAP analysis showing element distribution.

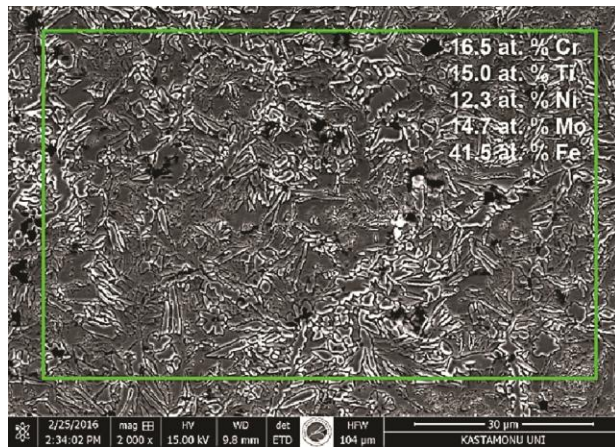


Fig. 4 — SEM images of the coating and EDS analysis.

analysis of CrFeNiMoTi HEA coating. The SEM image illustrates fairly homogeneous distribution of Fe, Cr, Ni, Ti and Mo in the coating layer. According to the image, the substrate entirely consisted of iron. Figure 4 shows SEM image and EDS analysis of HEA coating centre. Amounts of Cr, Ti, Ni and Mo elements in coating layer has almost the same value. However, the amount of Fe is significantly greater than the other elements because Fe element was diffused into the coating layer during the coating process.

Figure 5 shows some nano-scale precipitates in the coating. Several researchers^{15,16} pointed out that the simple solid solutions or nano-precipitates could easily form in the HEAs during solidification due to the high mixing entropy and sluggish cooperative diffusion of substitutional solute atoms. Therefore, difficulty in substitutional diffusion of alloying elements and interactions in interdiffusion during partitioning lowered the rates of nucleation and

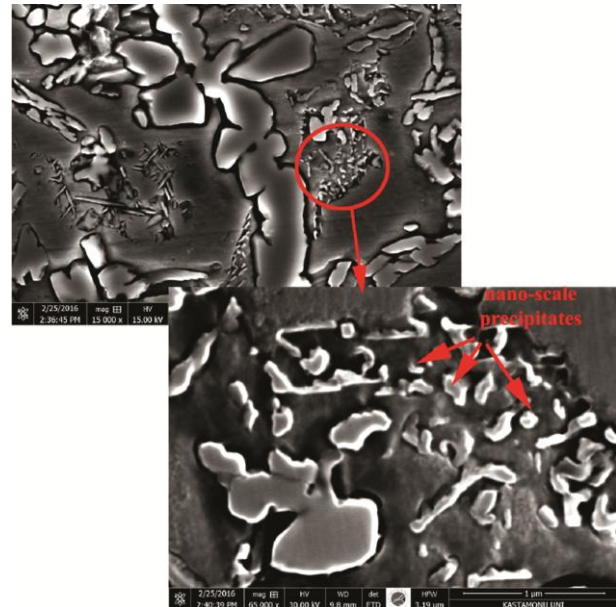


Fig. 5 — SEM images of formation of nanoprecipitates.

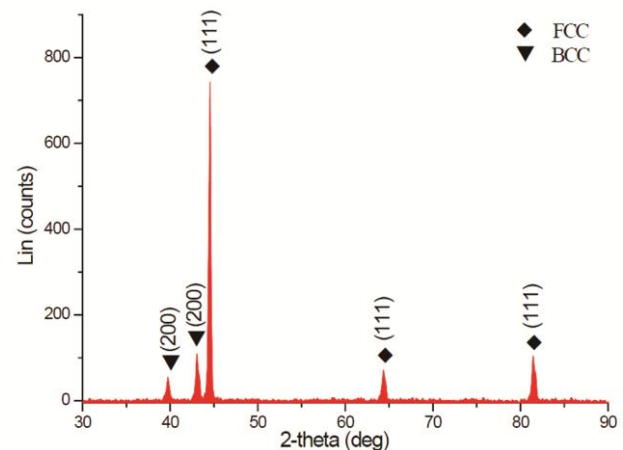


Fig. 6 — XRD patterns of the CrFeNiMoTi HEA coating.

growth, leading to the formation of nano-precipitates in the coating.

Figure 6 shows the X-ray diffraction patterns of the coatings. The phases in the CrFeNiMoTi coating could be identified as face-centred cubic (FCC) solid solution with diffraction peaks at about $2\theta=44.0^\circ$, 64.0° and 81.5° and body-centred cubic (BCC) solid solution with diffraction peak at about $2\theta = 39.5^\circ$ and 42.8° . Thus, Fe, Cr, Ni, Ti, and Mo elements are expected to distribute in the supersaturated solid solutions.

3.2 Microhardness

Figure 7 shows the micro-hardness distribution ranging from AISI 1040 steel substrate to the surface

of the coatings. The average thickness of the coating was about 1.6 mm. The average hardness value of the coating was 450 HV_{0.3}. The microhardness of the coating was higher than the steel (200 HV_{0.3}). Its reasons could be the grain refinement, nano-precipitates and increased solubility limitation in the coating due to the rapid cooling rate in TIG process.

3.3 Wear

Figure 8 shows wear graphs of the substrate and the coating specimen. While coefficients of friction ranged between 0.652-0.785 depending on the load applied for the substrate, this value varied in range of 0.386-0.523 for the coating specimen. As it is understood from these values, coefficient of friction substantially decreased as a result of coating AISI

1040 steel with CrFeNiMoTi alloy. The coefficient of friction in range of 10 N-15 N decreased for the substrate. This situation was caused by tribolayer occurring on specimen surface during the wear process. The coefficient of friction increased in the range of 15 N-20 N. This increase can be explained by the fact that there was more contact area between worn material and counter material thanks to load increase and consequently zonal low temperature increases occurred¹⁷. An increase was observed in friction coefficient of the coating layer in linear to load increase.

According to Archard’s law, wear resistance of the materials showed a property parallel to hardness of the material. In this study, HEA coating layer increased hardness of the substrate. Herewith, an increase occurred in also wear resistance. The wear resistance was interpreted as a criterion of wear rates. The wear rate was calculated by using the following formula¹⁸:

$$\text{Specific wear rate} = \frac{V}{WL} \quad \dots(1)$$

where, V is the volumetric wear loss, W is the applied load, and L is the wearing (sliding) distance. Wear losses was determined by using surface profilometer. As is seen in Fig. 8, wear rates increased depending on the load applied for both the substrate and the coating layer. While worn material was exposed to plastic deformation over against counter material under low loads, micro fractures, rupture of

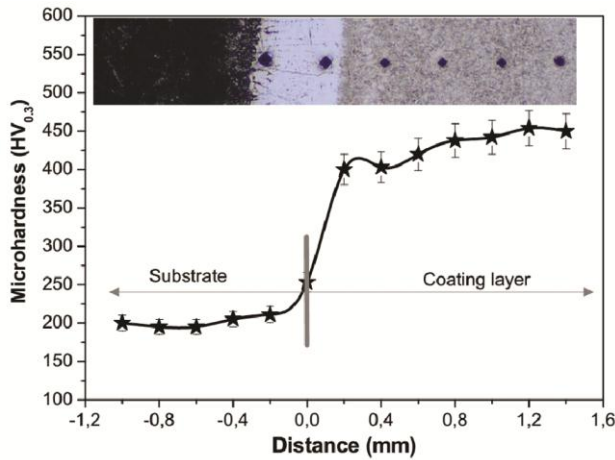


Fig. 7 — Micro-hardness distribution for coating/substrate.

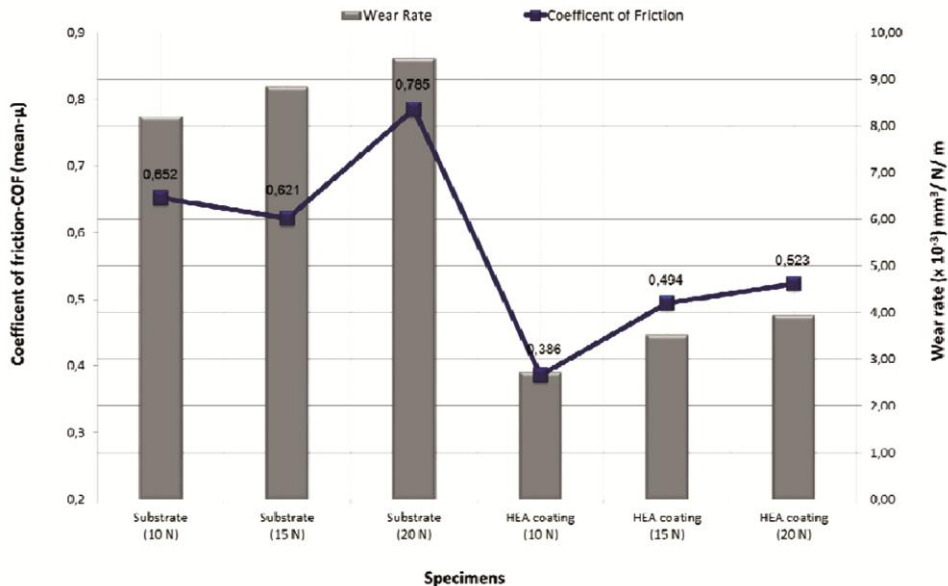


Fig. 8 — Wear rate and COF graph of specimens.

hard phases form matrix, and fragmentation occurred in the structure of material with increasing load. Based on the level of load, rate of this damage increased as well. While wear rate ranged between $\sim 8.215 \times 10^{-3} \text{ mm}^3/\text{N/m}$ and $\sim 9.455 \times 10^{-3} \text{ mm}^3/\text{N/m}$ for the substrate, this value ranged between $\sim 2.732 \times 10^{-3} \text{ mm}^3/\text{N/m}$ and $\sim 3.952 \times 10^{-3} \text{ mm}^3/\text{N/m}$ for the coating layer.

Figure 9 shows wear profile graph and images obtained by using surface profilometer device from surface of worn specimens following wear process. According to the graph, it was very obvious that wear loss of the substrate was higher compared to the coating layer. While wear depth of the substrate was respectively $\sim 15 \mu\text{m}$, $\sim 32 \mu\text{m}$ and $\sim 45 \mu\text{m}$ depending on 10 N, 15 N, and 20 N loads, these values for coating layer were, respectively $\sim 6 \mu\text{m}$, $\sim 17 \mu\text{m}$, and $\sim 37 \mu\text{m}$ for the coating layer (Fig. 9a). The same situation was seen from profile images in Fig. 9b and c.

Figure 10 shows morphologies of worn surfaces of the substrate and the coating layer under different loads. Both adhesive and abrasive wear type were dominant on substrate and coating layer. Material loss of the substrate after wear occurred in the form of channels of intensive plastic deformation and micro

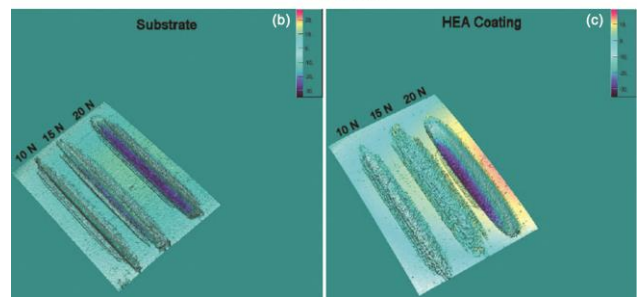
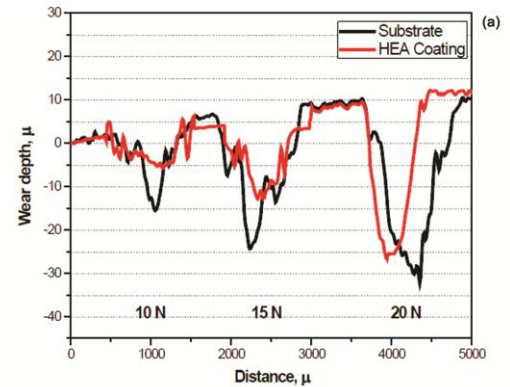


Fig. 9 — Optical profilometry images of a series of wear tracks for substrate and coating, at different applied loads (a) Line-scan type plot, (b) Pseudo three-dimensional plot of substrate, and (c) Pseudo three-dimensional plot of HEA coating.

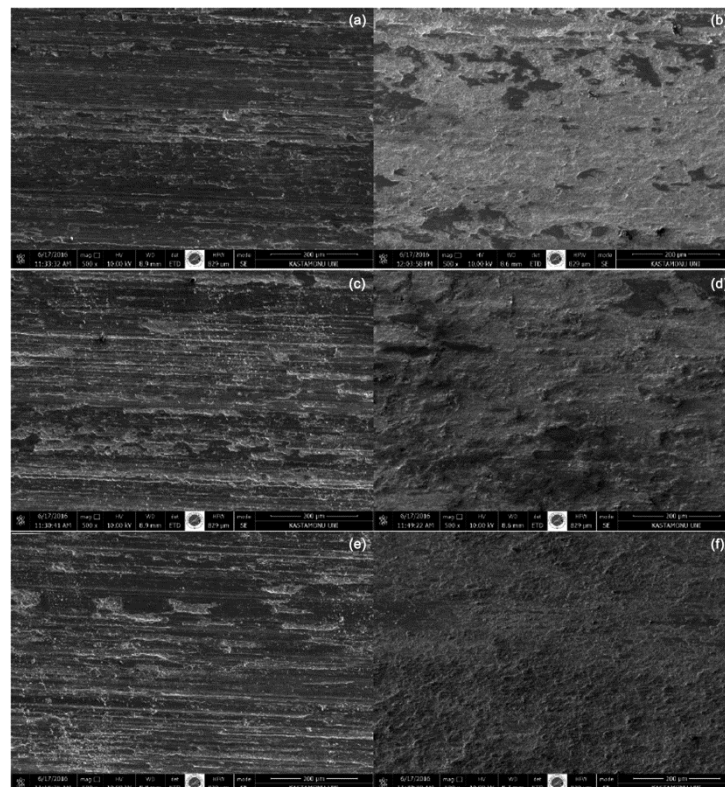


Fig. 10 — Worn surface morphology of substrate under loads of (a) 10 N, (b) 15 N, (c) 20 N and of the HEA coating under loads of (d) 10 N, (e) 15 N and (f) 20 N.

Table 1 — EDS analysis of worn surface of substrate and HEA coating after wear test under 20 N load (wt.%).

Specimens	Fe	C	Mn	O	Cr	Ni	Ti	Mo
Substrate	78.74	0.38	1.77	19.11	-	-	-	-
HEA coating	47.30	0.08	-	12.78	10.56	9.82	11.44	8.02

ploughing and leastwise wedge formation (Fig. 10 (a-c)). Plastic deformation and micro ploughing on wear surface of the coating layer were almost nonexistent. The reason for this was associated wear rate resulting from hard coating layer and low friction coefficient. This caused the coating layer to become scratch resistant against plastic deformation, counter material, and wear products. In contrast to the substrate, adhesive wear was higher in coating layer compared to abrasive wear. Formation of wear grooves was less. Material loss of coating layer occurred more as a result of wedging and delamination wear (Fig. 10 (d-f)). Losses observed for both specimens increased further with increasing load. Table 1 shows EDS analysis of wear surface of both substrate and coating layer which were exposed to 20 N of load. Oxide formation occurred in both specimens. Oxide layer contributed the decrease of friction coefficient by showing tribolayer effect. This layer ruptured under high loads and caused formation of wear mechanisms with 2 objects and 3 objects.

4 Conclusions

- (i) A high-entropy alloy (HEA) coating with nominal composition of CrFeNiMoTi was prepared by using TIG process.
- (ii) The microstructure of the coating was mainly composed of partially dendritic structure. Besides, nano-scale precipitates formed in the coating.
- (iii) XRD results showed that CrFeNiMoTi HEA coating were composed of mixed fcc/bcc phases.
- (iv) The hardness of CrFeNiMoTi HEA coating was much higher compared to the AISI 1040 steel substrate. The average hardness value was 450 HV_{0.3} for the coating.

(v) Wear tests showed that the wear resistance of AISI 1040 steel significantly improved after TIG clad CrFeNiMoTi HEA coating. Depending on the load, the wear rate and COF of the coating were much lower compared to AISI 1040 steel substrate.

References

- 1 Zhang Y, Zuo T T, Tang Z, Gao M C, Dahmen K A, Liaw P K & Lu Z P, *Progress Mater Sci*, 61 (2014) 1.
- 2 Zhang H, Wu W, He Y, Li M & Guo S, *Appl Surf Sci*, 363 (2016) 543.
- 3 Li J, Jia W, Wang J, Kou H & Zhang D, Beaugnon E, *Mater Des*, 95 (2016) 183.
- 4 Li Q H, Yue T M, Guo Z N & Lin X, *Metall Mater Transac A*, 44 (2013) 1767.
- 5 Zhang D W & Lei T C, *Wear*, 255 (2003) 129.
- 6 Pang W, Man H C & Yue T M, *Mater Sci Eng A*, 390 (2005) 144.
- 7 Islak S, Kır D, Buytoz S, Özorak C, Akkaş M, Çalgılı U & Yıldırım M M, *Pamukkale University J Eng Sci*, 21 (2015) 344.
- 8 Kumar S, Mondal D P & Jha A K, *J Mater Eng Perform*, 9 (2000) 649.
- 9 Buytoz S, Orhan A, Gur A K & Caligulu U, *Arabian J Sci Eng*, 38 (2013) 2197.
- 10 Islak S, Özorak C, Sezgin C T & Akkaş M, *Arch Metall Mater*, 61 (2016) 1515.
- 11 Cao Y, Zhi S, Gao Q, Tian X, Geng T, Guan X & Qin C, *Mater Character*, 119 (2016) 159.
- 12 Islak S, Buytoz S & Karagöz M, *Indian J Eng Mater Sci*, 19 (2012) 253.
- 13 Buytoz S & Ulutan M, *Surf Coat Technol*, 200 (2006) 3698.
- 14 Lin Y C & Wang S W, *Tribology Int*, 36 (2003) 1.
- 15 Tong C J, Chen Y L, Yeh J W, Lin S J, Chen S K, Shun T T, Tsau C H & Chang S Y, *Metall Mater Transac A*, 36 (2005) 881.
- 16 Zhang H, Pan Y & He Y, *Mater Des*, 32 (2011) 1910.
- 17 Stewart T L & Plucknett K P, *Wear*, 318 (2014) 153.
- 18 Zhou F, Wang Y, Liu F, Meng Y & Dai Z, *Wear*, 267 (2009) 1581.